

MAXIMALLY DUSTY STAR-FORMING GALAXIES: SUPERNOVA DUST PRODUCTION AND RECYCLING IN LOCAL GROUP AND HIGH-REDSHIFT GALAXIES

C. GALL¹ AND J. HJORTH¹

¹*Dark Cosmology Centre, Niels Bohr Institute, University of Copenhagen, Juliane Maries Vej 30, DK-2100 Copenhagen, Denmark*

ABSTRACT

Motivated by recent observations suggesting that core-collapse supernovae may on average produce $\sim 0.3 M_{\odot}$ of dust, we explore a simple dust production scenario which applies to star-forming galaxies in the local environment (the Magellanic Clouds and possibly the Milky Way) as well as to high redshift (sub- millimeter, QSO, Lyman break) galaxies. We assume that the net dust destruction (due to supernova reverse shock, shocks in the interstellar medium, or astration) is negligible on a timescale of 1 Gyr, in which case the dust mass can be estimated as 0.004 times the star-formation rate (for a Chabrier IMF) multiplied by the duration of the star-formation episode. The model can account for observed dust masses over four orders of magnitude and across the redshift range 0–8.4, with dust production rates spanning five orders of magnitudes. This suggests that star-forming galaxies may be seen as maximally dusty, in the sense that a dominant fraction of the dust-forming elements forged in a supernova eventually will go into the solid phase. In turn, this indicates little destruction of supernova dust or almost complete replenishment, on a short time scale, of any dust that is destroyed.

Keywords: dust, extinction — galaxies: high-redshift — galaxies: star formation — Local Group — supernovae: general

1. INTRODUCTION

A popular picture of cosmic dust production stipulates that asymptotic giant branch (AGB) stars are major producers of dust and/or provide the seeds for subsequent growth in molecular clouds or the interstellar medium (ISM) through accretion to reach the levels of dust observed in most galaxies (e.g., [Draine 2009](#); [Hirashita 2012](#)). However, recent observations challenge this scenario. In particular, the large dust masses found in high-redshift QSOs (e.g., [Wang et al. 2008](#); [Michałowski et al. 2010c](#); [Marrone et al. 2018](#)) cannot be accounted for by AGB star dust formation because of the limited time available since the Big Bang ([Dwek et al. 2007](#); [Gall et al. 2011c](#)). In parallel, closer to home, [Matsuura et al. \(2009\)](#) pointed out a ‘missing dust-mass problem’ in the Large Magellanic Cloud (LMC) arising from the inability of existing AGB stars to produce the dust mass observed in the ISM. A similar problem exists in the Milky Way (MW) ([Draine 2009](#)) and the Small Magellanic Cloud (SMC) ([Boyer et al. 2012](#); [Matsuura et al. 2013](#)). Moreover, the dust emission in the LMC and SMC appears to trace the ISM gas rather than the stellar content of the galaxies ([Meixner et al. 2013](#)). Thus, in the Local Group, AGB and red supergiant stars appear to directly contribute only a maximum of 5–10% to the total dust budget.

Current literature is surprisingly divided regarding the origin of cosmic dust. For example, there are claims that AGB stars ([Valiante et al. 2011](#); [Boyer et al. 2012](#)), supernovae (SNe) ([Gall et al. 2011b,c](#); [Ferrara et al. 2016](#)) or grain growth in molecular clouds ([Draine 2009](#); [Michałowski et al. 2010a,b](#); [Hirashita 2012](#)) are the prime sources. Fairly advanced chemical evolution models (see, e.g., [Dwek 1998](#); [Calura et al. 2008](#); [Zhukovska et al. 2008](#); [Gall et al. 2011a,b](#); [Rowlands et al. 2014](#); [Michałowski 2015](#); [Popping et al. 2017](#)) or large scale low resolution cosmological simulations ([McKinnon et al. 2017](#); [Aoyama et al. 2018](#)) are often used as tools to describe the complex physics and astrophysics of the life cycle of cosmic dust. The differing conclusions reached suggest that the outputs of such models, in part, reflect the physical prescriptions adopted for the formation, transformation, and destruction of dust as well as the input parameters chosen, such as the assumed net dust productivity of SNe. Furthermore, while the number of measured parameters of a galaxy is often limited to a handful (such as the dust mass, the stellar mass, the star formation rate, the metallicity, or the dust-to-gas ratio), chemical evolution models easily comprise several dozens of unknown or uncertain parameters, some of which may potentially strongly impact the final conclusions.

In this paper we investigate a simple unifying scenario in which core-collapse SNe are hypothesized to be responsible, directly or indirectly, for producing the majority of the dust in high-redshift star-forming massive galaxies, as well as the

SMC, the LMC, and possibly even the MW ([McKinnon et al. 2016](#)). To set the stage, we discuss the state-of-the-art picture of SN dust production and destruction as well as grain growth in the dense ISM in Section 2 (this Section can be skipped from a cursory reading). We next develop a model involving only few parameters and use recent measurements of the amount of dust produced by SNe in Section 3. We present existing observational constraints on Local Group galaxies as well as high-redshift dusty galaxies in Section 4 and discuss the results in Section 5.

Our analysis shows that SNe can barely produce all the dust provided that none of the newly formed SN dust is destroyed. Alternatively, dust has to reform about as quickly as it was formed in the first place and not be prone to subsequent destruction by the processes, which destroyed the original SN dust. In this sense, (dusty) galaxies can be seen as maximally dusty. This result is illustrated in Figure 3 which relates observed dust masses to those estimated from Equation 1 in Section 3.

2. STATE OF THE ART: SN DUST PRODUCTION, DESTRUCTION AND GRAIN GROWTH

Massive stars and core-collapse SNe are known to produce dust (e.g., [Cernuschi et al. 1967](#); [Hoyle & Wickramasinghe 1970](#); [Clayton 1979](#); [Kozasa et al. 1989](#); [Wooden et al. 1993](#); [Todini & Ferrara 2001](#); [Nozawa et al. 2003](#); [Pozzo et al. 2004](#); [Barlow et al. 2005](#); [Smith et al. 2008](#); [Fox et al. 2009](#); [Kotak et al. 2009](#); [Cherchneff & Dwek 2010](#); [Kochanek 2011](#); [Smith 2012](#); [Sarangi & Cherchneff 2013](#), see review by [Gall et al. 2011c](#)). The main issues regarding this scenario are: do core-collapse SNe produce sufficient amounts of dust and will what they produce survive the transit into the ISM ([Gall et al. 2011c](#)) and subsequent destruction in the ISM ([Jones & Nuth 2011](#); [Slavin et al. 2015](#)).

2.1. SN dust production

A discussion of dust masses inferred from SNe is provided by [Gall et al. \(2011c, 2014\)](#). While many measurements and lower limits are available at early times, few accurate measurements have been made at late times, uncontaminated by intervening sources. Figure 1 is a compilation of reported dust masses in SNe and SN remnants as a function of time since explosion. It is an extended version of Figure 4 in [Gall et al. \(2014\)](#), updated with the latest dust mass measurements of SNe and supplemented with masses of older SN remnants, including the 10000 yr old SN remnant Sgr A East ([Lau et al. 2015](#)), which has warm ($\gtrsim 100$ K) dust mass measurements. These measurements demonstrate that substantial amounts of dust (of order $0.1\text{--}1 M_{\odot}$) can be produced, consistent with most theoretical estimates ([Todini & Ferrara 2001](#); [Nozawa et al. 2003](#); [Cherchneff & Dwek 2010](#)). Detailed modeling of existing data suggests that dust mass either increases over

time (Gall et al. 2014; Wesson et al. 2015), as suggested by Figure 1, or is formed instantly at early times in optically thick clumps (Dwek & Arendt 2015).

Only three SNe, SN 1987A, SN 1054 (Crab), and Cas A have had their dust masses measured accurately. A large dust mass in SN 1987A was first inferred by Matsuura et al. (2011) based on *Herschel* data, later confirmed using ALMA observations (Indebetouw et al. 2014; Matsuura et al. 2015). Based on *Herschel* and *Planck* data, Gomez et al. (2012) detected significant dust emission from the Crab nebula (see also Temim & Dwek 2013; Owen & Barlow 2015; Mattsson et al. 2015). Dust has been detected in the Cas A (Dunne et al. 2003, 2009; Barlow et al. 2010) and N49 (Otsuka et al. 2010) SN remnants but in these cases it is challenging to distinguish dust formed by the SN, interstellar dust, or foreground dust. De Looze et al. (2017) recently managed to overcome this challenge for Cas A.

Core-collapse SNe interacting with their circumstellar material have also been shown to be dust producers (Smith et al. 2008; Mattila et al. 2008; Kotak et al. 2009; Meikle et al. 2011; Gall et al. 2014). Finally, massive progenitors of SNe, such as luminous blue variable stars, also appear to produce dust with a standard dust-to-gas ratio (Smith 2012). For example, about $0.4 M_{\odot}$ of dust within 2×10^{17} cm has been inferred in the massive erupting star, η Car (Gomez et al. 2010; Morris et al. 2017). Such dust is usually assumed to be evaporated by the shock breakout radiation from the ultimate supernova explosion, but dust at sufficiently large radius may possibly survive, depending on the details of the shock breakout radiation.

2.2. SN reverse shock dust destruction

The expanding forward shock resulting from the SN explosion sweeps up any circumstellar and interstellar material, ultimately leading to the creation of a reverse shock (e.g., Chevalier 1977). The presence or absence of substantial circumstellar material may influence the timescales of when the reverse shock interacts with the SN-formed (ejecta) dust. For example, using theoretical models which do not consider any circumstellar material, it has been suggested that a reverse shock, launched by the swept up interstellar material only, may destroy the majority of the dust produced by the SN, on time scales of $\sim 10^4$ years (for an ambient density $n \sim 0.1\text{--}10$ cm $^{-3}$, e.g., Bianchi & Schneider 2007). On the other hand, simulations of early reverse shocks in Type II_n SNe interacting with a dense circumstellar shell suggest that the reverse shock oscillates between layers of swept up material due to radiative cooling on timescales of tens of days, too short to affect newly formed dust but able to explain ripples in early lightcurves (Whalen et al. 2013).

In theoretical models (Bianchi & Schneider 2007; Micelotta et al. 2016; Bocchio et al. 2016; Biscaro & Cherchneff 2016)

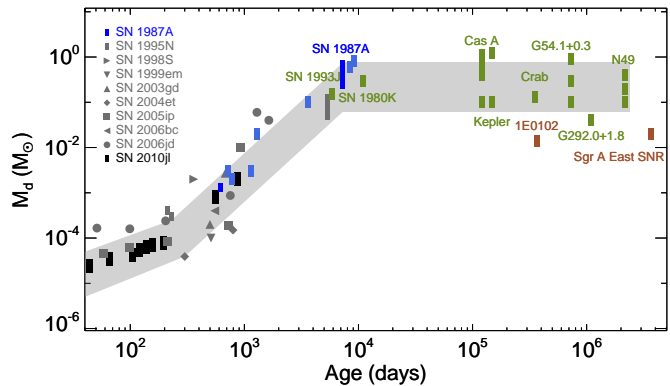


Figure 1. Supernova dust mass evolution. SN data indicated as grey and black symbols are taken from Gall et al. (2014, and references therein). Data for SN 1987A (Matsuura et al. 2015; Lawrence 2012; Indebetouw et al. 2014; Wesson et al. 2015; Bevan & Barlow 2016) are indicated as blue symbols. For these SNe, the age refers to the time past the maximum visual light. SN remnants (SNRs) with cold dust measurements are indicated as green bars (age here refers to the time past explosion), namely for SN 1993J and SN 1980K (Bevan et al. 2017), Cas A (Bevan et al. 2017; Arendt et al. 2014; De Looze et al. 2017), Kepler (Gomez et al. 2009), Crab (Gomez et al. 2012; Owen & Barlow 2015; Temim & Dwek 2013), G54.1+0.3 (Temim et al. 2017; Rho et al. 2017), G292.0+1.8 (Ghavamian & Williams 2016) and N49 (Otsuka et al. 2010). Red bars mark SNRs with warm dust ($\gtrsim 100$ K) measurements for 1E0102 (Rho et al. 2009) and Sgr A East SNR (Lau et al. 2015). The grey area between 40 and 7305 days illustrates a possible trend of dust formation, while the grey area from 7305 days to 3000 years reflects the scatter ($0.34 M_{\odot}$ rms) around the mean value of $0.40 \pm 0.07 M_{\odot}$ of the SNRs within this period.

the properties of the reverse shock (e.g., Chevalier 1977) are often based on the formalism described in Truelove & McKee (1999) and references therein. Rather different conclusions regarding the effect of the reverse shock are reached. For example, Nozawa et al. (2007) find large survivability rates while Bianchi & Schneider (2007) find a large destruction rate. These rates depend on the assumed destruction mechanisms as well as the morphology of the SN remnant and surrounding material.

Part of the discrepancy can also be traced back to the input model of the dust grain size distribution. Thus, models which consider either large grains or dust residing in dense ejecta clumps, lead to survival rates in the range 40–98 % (Silvia et al. 2010, 2012; Biscaro & Cherchneff 2016; Nath et al. 2008), while, depending on the ambient density, only $\lesssim 2\text{--}20$ % survives in models with very small grains (Bianchi & Schneider 2007; Mancini et al. 2015; Micelotta et al. 2016; Bocchio et al. 2016).

Other mechanisms may significantly alter the effects of reverse shock interaction with the SN formed dust. ISM magnetic fields may lead to dust grains being trapped in the heart of a SN remnant (Fry et al. 2018). In models taking dust

charge and magnetic fields into account, dust filaments may be created by non-linear manifestations of highly-supersonic resonant drag instabilities (Hopkins & Squire 2018). Such filaments could drift through the reverse shock, thereby possibly avoiding effects of the reverse shock entirely. From an observational perspective, the detection of about $0.02 M_{\odot}$ of warm dust (~ 100 K) in the ~ 10000 year old SN remnant Sagittarius A East in the Galactic center suggests that there is limited dust destruction due to the reverse shock (Lau et al. 2015).

Reverse shocks in SNe and SNRs have also been detected on much shorter timescales, i.e., of order tens or hundreds of years. SN 1998S exhibited reverse shock emission after 14 years, at which point significant amounts of dust was reported in the unshocked ejecta inside the reverse shock as well as in the CSM, outside the reverse shock (Mauerhan & Smith 2012). Ongoing reverse shock activity has also been detected in the outer shell of SN 1987A (Sonneborn et al. 1998; France et al. 2011; Fransson et al. 2013), in Cas A (Morse et al. 2004; Wallström et al. 2013) and in SN 1006 (Winkler et al. 2011). There are also indications of ejecta dust in other decades-old SNe (Milisavljevic et al. 2012), although it is unclear to what extent the remnants have been affected by a reverse shock. On the other hand, so far no such activity has been seen in the ~ 1000 year old SN 1054 (the Crab nebula), where the dust seems to be shielded in dense filaments and well set to begin its transit into the ISM (Gomez et al. 2012).

In summary, it is at present unclear to what extent the SN produced dust will survive the destruction by the various short and long time-scale reverse shocks.

2.3. SN forward shock ISM dust destruction

A SN forward shock can strongly affect the existing dust in the CSM or ISM. A variety of physical processes are at work, ranging from shattering, which affects the grain size distribution, to destructive processes, such as sputtering or vaporization, which decrease the total dust mass (e.g., Barlow 1978; Jones et al. 1996; Slavin et al. 2004). These destruction processes apply to any kind of dust, not just dust produced by SNe.

Ongoing dust destruction of swept up ISM dust grains has been seen in the SNRs N49 (Dopita et al. 2016) and Puppis A (Arendt et al. 2010). The observations suggest that about 30–90 % of the Fe-bearing grains around N49 and about 25% of the graphite and silicate dust around Puppis A is destroyed. About 35% of the mass of grains are destroyed inside a 0.14 pc region behind the forward shock of the Cygnus Loop SNR (Sankrit et al. 2010).

Lakićević et al. (2015) and Temim et al. (2015) found very large destruction rates of SNe from studies of SN remnants in the Magellanic Clouds. They concluded that there is less dust

inside the SN remnant, implying a very large destruction rate and a very short dust survival time.¹ These works suggest that SNe destroy more dust than they form, and hence would imply that SNe should in principle destroy all dust on very short time scales, 20–50 Myr. Destruction time scales shorter than injection time scales (60 Myr) for Si-bearing grains in the ISM were also found by Tielens (1998). Other estimated time scales are longer, of order 100 Myr (Jones & Nuth 2011) or 1000 Myr for the SMC (Matsuura et al. 2013).

Very short destruction time scales could imply that dust would not be present in most galaxies. It has therefore been suggested that SNe cannot be allowed to be efficient dust destroyers if we are to observe the dust we see in galaxies (Gall et al. 2011a,b; Hjorth et al. 2014). As in the case of the reverse shock models, the dust composition and grain size distribution as well as the morphology of the ISM are important. Recent estimates of ISM dust destruction time scales have gone up significantly, to ~ 2 –3 Gyr for (small grain) silicates (Slavin et al. 2015). These models consider that SN dust destruction is efficient only in the warm phase of the ISM, which in the work by Slavin et al. (2015) is assumed to make up 80% of the ISM. The time scales increase because dust destruction in the cold and hot phases of the ISM may be inefficient (Slavin et al. 2015) and are also enhanced for larger grains or a lower filling factor of the warm ISM as larger grains are more robust (e.g., Silvia et al. 2010).

Clustered SN explosions, as opposed to isolated SN explosions, can cause a net increase in the amount of dust in the surroundings of young massive stellar clusters (Martínez-González et al. 2018). At small SN shock destruction rates (i.e., for masses of ISM gas cleared of dust by a single supernova remnant of less than about $100 M_{\odot}$), dust destruction will dominate the dust destruction in galaxies (Hjorth et al. 2014).

2.4. Grain growth in the dense ISM

Dust grains can grow through accretion of ions in the ISM such as in dense molecular clouds or in the cold neutral medium (e.g., Draine 2009). This process is often invoked in the Milky Way (Draine 2009; Hirashita 2012; Zhukovska et al. 2016) and more generally at high redshift (e.g., Michałowski et al. 2010c), especially in scenarios in which SNe are assumed to be net destroyers of dust because of catastrophic reverse shock destruction and forward shock

¹ We note that the formal significance of the Lakićević et al. (2015) results is marginal and may be affected by warm dust preventing any cold dust present to be detected (Micelotta et al. 2018). The short dust lifetimes obtained by Temim et al. (2015) are based on the formalism of Dwek et al. (2007) to calculate SN dust destruction efficiencies as a function of SN shock velocity. We note that the analysis assumes small grains and 100 % destruction at shock velocities of 500 km/s, at variance with the observations of Puppis A suggesting destruction of up to 25 % of the grains at such velocities (Arendt et al. 2010).

destruction of pre-existing ISM dust. Simple grain growth models often consider spherical grains and assume that all accreted atoms stick onto the grains, thereby increasing the mass of grains, possibly yielding rapid accretion time scales of $\lesssim 1$ Myr (e.g., Hirashita 2012), depending sensitively on the density of the medium, the type of ion, and the sizes of the seed grains.

Chemical evolution models typically treat grain growth in a parametrized way primarily determined by the amount of gas phase metals instantly mixed into an estimated number of clouds with assumed physical conditions (lifetimes, temperatures, densities) similar to those in the Milky Way (e.g., Draine 2009; Valiante et al. 2011; Pipino et al. 2011; Asano et al. 2013; Calura et al. 2014; Mancini et al. 2015; Popping et al. 2017; Ginolfi et al. 2018).

While grain growth in cold (a few tens of K) dense molecular clouds in the Milky Way is an important (but slow) process, the physical conditions in massive starburst galaxies is likely far from similar to those in the Milky Way (Ceccarelli et al. 2018). Indeed, Ferrara et al. (2016) point out that at high redshift the higher CMB temperature ($T_{CMB}=2.725(1+z)$) prevents dust to cool to temperatures ($\lesssim 20\text{--}30$ K) required for particles to stick to the surfaces of seed grains, hampering efficient grain growth. Additionally, dust growth in cold molecular clouds largely proceeds through the coating of refractory seed grains with icy mantles composed of primarily water ice and some molecules such as, e.g., NH_3 , CO , CO_2 and more complex ones (Caselli & Ceccarelli 2012; Boogert et al. 2015) through hydrogenation and oxidation of atoms and simple molecules on the surfaces of grains. Dust forming elements such as, e.g., Si, or C are at best embedded as impurities. While ice mantles possibly foster coagulation processes in cold molecular clouds (Boogert et al. 2013) on times scales of 10^7 yr (Ormel et al. 2009), rapid and efficient grain growth through accretion processes, however, is uncertain. For example, Ceccarelli et al. (2018) found that grain growth of Si-bearing grains through accretion of elemental Si remains impossible at any redshift.

Additionally, the lifetimes of giant molecular clouds is short, of order 4–25 Myr (Dobbs & Pringle 2013; Baba et al. 2017) and smaller dense molecular clumps, such as the birth places of massive stars in the LMC, may only live for less than 1 Myr (Seale et al. 2012). The mixing time scales may also be longer than ‘instant’, up to 125–350 Myr for massive galaxies (de Avillez & Mac Low 2002; Krumholz & Ting 2018). Longer mixing timescales may cause an imbalance between metal production and diffusion, which possibly explains the large diversity of metallicity distributions in high redshift galaxies (Petit et al. 2015).

On the other hand, metal depletion studies show that up to 99% of all the iron ejected by core collapse SNe or SNe Ia is depleted in the various temperature phases of the ISM of

local as well as higher redshift galaxies (Jenkins 2009; De Cia et al. 2016). Elemental depletion patterns have been suggested to be a signature of grain growth in the ISM through accretion of ions onto pre-existing grains (Dwek 2016; De Cia et al. 2016; Zhukovska et al. 2018). The large depletion rates of iron combined with the lack of evidence for dust formation by SNe Ia (e.g., Gall et al. 2011c; Nittler et al. 2018, and references therein), which produce a dominant fraction of the iron in the universe, suggests that a substantial fraction of the iron must be incorporated in dust grains grown in the ISM. Conversely, the detection of crystalline silicates are hard to reconcile with dust grown in the ISM (Dwek 2016).

3. ESTIMATING THE DUST MASS DUE TO SUPERNOVAE IN A STAR-FORMING GALAXY

In this section we develop a simple model for the dust mass in a galaxy with a given (simple) star-formation history. For a star-forming galaxy, we estimate the total dust mass produced by SNe by making the following assumptions:

- The dust is produced during a star-formation episode of duration Δt with a mean star-formation rate ψ .
- The life times of dust-producing massive stars are negligible compared to Δt .
- The rate of SNe (i.e., of massive stars) is proportional to the star-formation rate, i.e., $\gamma\psi$.
- Massive stars (SNe and their progenitors) on average produce η solar masses of dust.
- On time scales shorter than Δt , the net growth or destruction of dust in the ISM is negligible.

Under these assumptions the resulting dust mass is proportional to the average star-formation rate during the star-formation episode,

$$M_d = \mu_D \psi \Delta t, \quad (1)$$

with

$$\mu_D \equiv \gamma \eta, \quad (2)$$

(see also Gall et al. 2011c; Hjorth et al. 2014, whose notation we adopt in this paper). With this definition, the dust production rate is simply

$$DPR \equiv \frac{M_d}{\Delta t} = \mu_D \psi. \quad (3)$$

In the remainder of this Section we discuss the values and uncertainties of the parameters entering these expressions.

3.1. The proportionality factor between star-formation rate and SN rate, γ

The number of core-collapse SNe produced per gas mass available for star formation is

$$\gamma \equiv \frac{\int_{8 M_{\odot}}^{40 M_{\odot}} \phi(m) dm}{\int_{m_{\min}}^{100 M_{\odot}} \phi(m) m dm}. \quad (4)$$

Here, the stellar initial mass function (IMF), $\phi(m)$, is defined as the number of stars, $\phi(m)dm$, in the mass interval m to $m+dm$, where m is the zero age main sequence mass. The IMF directly determines the number of massive stars exploding as SNe relative to the total mass of stars. It is defined over the range $m_{\min} < m < 100 M_{\odot}$, with $0.1 M_{\odot} \leq m_{\min} < 8 M_{\odot}$. The mass range for core-collapse SN formation is traditionally taken to be $8 M_{\odot} < m < 40 M_{\odot}$ (Heger et al. 2003; Ibeling & Heger 2013). The Salpeter IMF, which takes a power-law form,

$$\phi(m) \propto m^{-\alpha}, \quad (5)$$

with $\alpha = 2.35$, results in $\gamma = 0.007 M_{\odot}^{-1}$.

It is known that the total SN dust production depends on the IMF (Dwek et al. 2007; Gall et al. 2011c; Hjorth et al. 2014), in particular through γ . However, so does the total inferred star-formation rate. As long as the star formation rate is inferred consistently with the same IMF as that used to infer γ then our results will be largely independent of the adopted IMF because we will correctly infer the number of massive stars (and hence dust producing SNe; note however that a starburst can be sustained for longer for an IMF disfavouring low-mass stars). Therefore, in this paper we assume a Salpeter IMF and convert reported Chabrier IMF based values to Salpeter IMF values using a conversion factor of 1.8. IMF-independent massive star-formation rates can be obtained by dividing the Salpeter IMF SFR by 10.

Strolger et al. (2015) compared measured volumetric core-collapse SN rates to the observed cosmic SFR density (for a Salpeter IMF Madau & Dickinson 2014). The inferred value of $\gamma = 0.0091 \pm 0.0017 M_{\odot}^{-1}$ suggests that we adopt a 0.15 dex uncertainty in γ for a given IMF.

3.2. The average dust mass per core-collapse SN, η

In Figure 1 we have updated the evolutionary trend suggested by Gall et al. (2014) with recent SN dust mass measurements including SN remnants. It appears that the maximum amount of dust formed in a SN is reached within about 30 years and is not significantly altered for another 1000 years. Formally, the mean value reached at late times is $0.40 \pm 0.07 M_{\odot}$.

However, this value is based on a very heterogeneous set of reported measurements and individual systematic uncertainties are hard to quantify. To obtain a more reliable estimate, we here focus on the three systems alluded to in Section 2.1,

which have exquisite measurements, detailed modeling, and systematic errors under control. We adopt a dust mass of $0.6 \pm 0.3 M_{\odot}$ for SNe 1987A. In the case of SN 1054 a dust mass of $0.15 \pm 0.12 M_{\odot}$ is consistent with all reported values (see Section 2.1 for references). Finally, De Looze et al. (2017) recently obtained a dust mass of 0.2–0.6 M_{\odot} in Cas A. The weighted mean of these three accurate observed dust mass yields is $0.26 \pm 0.10 M_{\odot}$ while the straight mean is $0.38 M_{\odot}$.

Such direct averages are likely to be biased since the three SNe may not be representative of the population of dust-producing core-collapse SNe. To compute an IMF-averaged mean dust mass we can compare to theoretical expectations and thereby take into account the distribution of progenitor masses.

We define the dust yield per SN as

$$\eta \equiv \frac{\int_{8 M_{\odot}}^{40 M_{\odot}} \epsilon(m) m_Z(m) \phi(m) dm}{\int_{8 M_{\odot}}^{40 M_{\odot}} \phi(m) dm}. \quad (6)$$

We use the analytical ‘maximum efficiency’ of Gall et al. (2011c),

$$\epsilon(m) \equiv \frac{m_d}{m_Z} = 1.2 \exp\left(-\frac{m}{13 M_{\odot}}\right), \quad (7)$$

which is an empirical expression derived from theoretical predictions of the dust mass per supernova (Todini & Ferrara 2001; Nozawa et al. 2003) which does not account for the effects of reverse shock dust destruction (e.g., Bianchi & Schneider 2007). Guided by the nucleosynthetic yields found by Woosley & Weaver (1995) and Umeda & Nomoto (2002) we assume the following expression for the metal production as a function of progenitor mass (see Figure 2),

$$m_Z(m) = \begin{cases} 0.01 \left(\frac{m}{M_{\odot}} - 8\right) m; & 8 < \frac{m}{M_{\odot}} < 30 \\ 0.22m; & 30 \leq \frac{m}{M_{\odot}} < 40. \end{cases} \quad (8)$$

With these expressions, we obtain an approximately linear relation between η and α ,

$$\eta/M_{\odot} \approx 0.314 - 0.106 (\alpha - 2.35), \quad (9)$$

independent of m_{\min} (see Figure 2). We note the excellent agreement between the observed and model dust yields depicted in Figure 2. We can therefore infer the expected IMF-averaged value of the dust yield per supernova to be $0.31 M_{\odot}$ to which we associate an uncertainty of 0.15 dex, see Figure 2. Combining the adopted values of γ and η we infer a dust productivity of $\mu_D = 0.0022$ (Gall et al. 2011c; Hjorth et al. 2014) for a Salpeter IMF or $\mu_D = 0.0040$ for a Chabrier IMF, with a ~ 0.2 dex uncertainty.

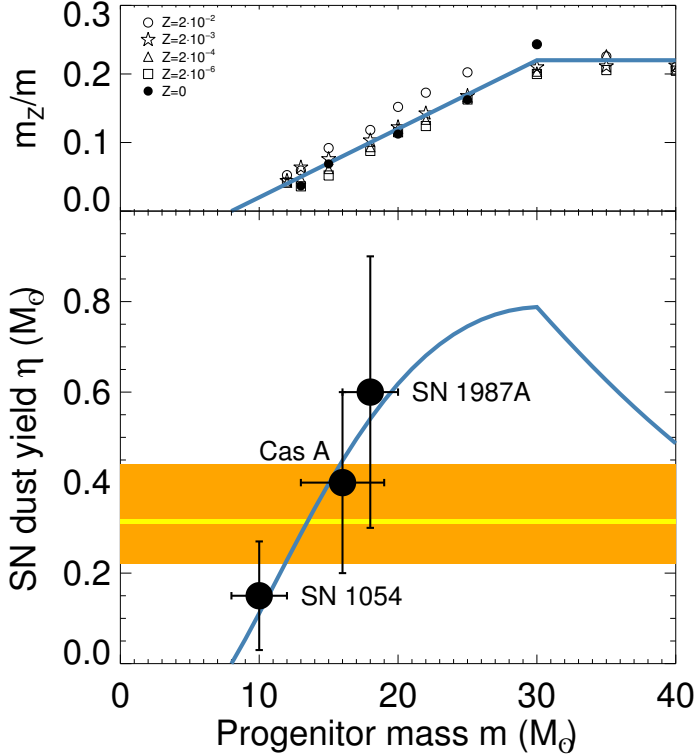


Figure 2. Lower panel: SN dust yield as a function of SN progenitor mass. The observed cold dust masses for the Crab (Gomez et al. 2012; Temim & Dwek 2013), SN 1987A (Matsuura et al. 2011; Indebetouw et al. 2014), and Cas A (De Looze et al. 2017) are plotted as filled black circles. The blue curve is a theoretical estimate of the SN dust yield (assuming no destruction) (adapted from Fig. 6 of Gall et al. 2011c using Equation 6). The IMF averaged dust yield is indicated as the yellow line for a Salpeter IMF. The orange band indicates the associated 0.15 dex error adopted. The average value is not strongly sensitive to the uncertain dust yield above $30 M_{\odot}$ due to the dominance of stars with lower masses. Upper panel: Relative metal production as a function of progenitor mass for different metallicities from Woosley & Weaver (1995) (open symbols) and Umeda & Nomoto (2002) (filled circle). The blue line is a representation of these points, as expressed in Equation (8).

3.3. The star-formation rate ψ

Observational SFR indicators are sensitive to possible dust extinction if inferred from the ultraviolet flux. Moreover, they strongly depend on the adopted IMF since the far-infrared or ultraviolet luminosity measures the massive SFR, while the extrapolation to total SFR depends on the relative number of lower-mass stars.

We adopt a 0.15 dex uncertainty in ψ for a given IMF, i.e., in the massive star-formation rate. We quote SFRs converted to Salpeter IMF and use a corresponding γ in computing SN rates. This way the results are independent of m_{\min} .

3.4. The duration of the star-formation episode Δt

Local Group galaxies have an extended star-formation history during which there will be time for AGB stars to contribute significantly to the dust mass budget (Schneider et al. 2014). There will also be growth of dust grains through accretion in the ISM. Conversely, destruction, astration and expulsion will counter these effects. Thus, Δt should be taken to be smaller than the time scales relevant to the latter processes. For the SMC, LMC and MW, Matsuura et al. (2013) estimated dust destruction time scales of 1.4 Gyr, 400 Myr and 500 Myr, respectively. These however were based on rather high estimates of the SN rates. Jones & Nuth (2011) estimate dust lifetimes of 0.1–1 Gyr in the ISM of the MW. We adopt a fiducial value at the upper end of this range, $\Delta t = 1$ Gyr, with a 0.3 dex uncertainty, whilst noting that dust destruction time scales are subject to current debate, see Section 5.

For massive starbursts at high redshift (e.g., sub-mm galaxies) it is likely that a large fraction of the dust observed is formed in the current burst. For starburst galaxies, the duration can be assessed from the observational data at hand and typically turns out to be of order 100 Myr. This is consistent with recent simulations which suggest that typical starbursts in galaxies at $z \sim 6$ have a duration of about 100 Myr (Ceverino et al. 2018), with more massive galaxies having slightly larger burst durations. In this paper we adopt $\Delta t = 100$ Myr for $z > 6$ galaxies while we adopt the slightly longer depletion time scale for sub-millimeter galaxies (SMGs) at $z \sim 3$.

In total, the combined uncertainty in our theoretical SN dust mass estimates is ~ 0.4 dex.

3.5. Observational dust mass estimates

There are significant uncertainties related to determining dust masses (Gall et al. 2011c). Far-infrared emission is usually interpreted as thermal dust emission. The temperature inferred from modified black body fits to the data is degenerate with the dust mass and significant amounts of cold dust could in principle be hidden and still be consistent with observational constraints. Other issues relate to the assumed type of dust, and hence the normalisation of the dust absorption coefficient κ and the emissivity index β (see, e.g., Michałowski et al. 2010a, for a discussion of observational uncertainties related to determining dust masses in SMGs and QSOs). We adopt an uncertainty of 0.4 dex in observed dust masses which matches the uncertainty in the dust mass inferred from the simple model.

4. DATA

For the purposes of illustrating the range of validity of our simple model, we here discuss the properties of the most prominent Local Group galaxies as well as a selection of representative high-redshift dusty galaxies. Table 1 summarizes

Table 1. Star Formation and Dust Properties

Galaxy	Redshift	ψ ($M_{\odot} \text{ yr}^{-1}$)	M_d ($10^6 M_{\odot}$)	Δt (Myr)
SMC	0	0.07	0.11	1000
LMC	0	0.2	1.1	1000
Milky Way	0	3.4	25	1000
SMGs	$\sim 2-3$	700	400	142
G09 83808	6.03	640	190	100
HFLS3	6.34	1190	300	100
QSO J1148+525	6.42	3000	590	100
SPT0311 E	6.90	972	400	100
SPT0311 W	6.90	5220	2500	100
A1689-zD1	7.5	49	50	100
MACS0416_Y1	8.31	25	4	180
A2744_YD4	8.38	37	5.5	100

NOTE—The star-formation rates are inferred assuming a Salpeter IMF with $m_{\min} = 0.1 M_{\odot}$. The horizontal lines delineate different object classes, namely Local Group galaxies, intermediate redshift SMGs, high-redshift SMGs, and high-redshift Lyman-break galaxies. These are plotted with different colors in Figure 3. For notes on individual objects, see Section 4.

the observational estimates of the star-formation rate and dust masses, as well as our adopted durations of the star-formation episode. The individual objects/object classes are discussed below.

The estimated current star-formation rate of the SMC is $3.7 \times 10^{-2} M_{\odot} \text{ yr}^{-1}$ (Bolatto et al. 2011), consistent with $0.03 M_{\odot} \text{ yr}^{-1}$ found by Skibba et al. (2012). The current value, however, is not directly relevant for our purposes because dust will have been built up over a longer period. Harris & Zaritsky (2004) inferred a burst of star formation lasting 200 Myr, about 400 Myr ago, at $0.25 M_{\odot} \text{ yr}^{-1}$. In a more recent study,²

Harris & Zaritsky (2009) find an average $0.18 M_{\odot} \text{ yr}^{-1}$ over 100 Myr (ranging from $0.1-0.3 M_{\odot} \text{ yr}^{-1}$), while the average over 10 Gyr is around $0.12 M_{\odot} \text{ yr}^{-1}$. Their high inferred current SFR of order $\sim 0.1 M_{\odot} \text{ yr}^{-1}$ suggests that we should use the lower boundary of the Harris & Zaritsky (2009) study. The average lower boundary over 200 Myr (left panel of their Fig. 19) is about $0.05 M_{\odot} \text{ yr}^{-1}$ while it is about

$0.07 M_{\odot} \text{ yr}^{-1}$ over the past 1 Gyr, which we adopt. We note that this could be a lower limit. Bot et al. (2010) estimated a dust mass of $0.29-1.1 \times 10^6 M_{\odot}$ from the measured sub-mm to cm excess. This could even be a lower limit if there is very cold dust. However, Skibba et al. (2012) (and references therein) argue that such a large dust mass would be inconsistent with the amount of metals available and instead quote a dust mass of $1.1 \times 10^5 M_{\odot}$, which we adopt (Leroy et al. 2007 find a dust mass of $3 \times 10^5 M_{\odot}$).

For the LMC, Harris & Zaritsky (2009) find that star formation has proceeded at an average rate of roughly $0.2 M_{\odot} \text{ yr}^{-1}$ for the past 5 Gyr. Skibba et al. (2012) find a dust mass of $1.1 \times 10^6 M_{\odot}$, which appears consistent with Matsuura et al. (2009) who quote a dust mass of $1.6 \times 10^6 M_{\odot}$, based on the gas mass and an assumed dust-to-gas mass ratio.

For the MW, Chomiuk & Povich (2011) find $\psi = 1.9 \pm 0.4 M_{\odot} \text{ yr}^{-1}$, calibrated to the Kroupa IMF. Correcting to Salpeter IMF (same correction factor as for the Chabrier IMF) gives $3.4 \pm 0.7 M_{\odot} \text{ yr}^{-1}$. Draine (2009) estimates the total amount of dust in the ISM as 0.005 times the mass in the ISM of $5 \times 10^9 M_{\odot}$, i.e., $M_d = 2.5 \times 10^7 M_{\odot}$.

SMGs and high-redshift QSOs typically have star-formation rates of order $1000 M_{\odot} \text{ yr}^{-1}$ and dust masses in the range $10^{8-9} M_{\odot}$ (Michałowski et al. 2010a,b; Gall et al. 2011b; Marrone et al. 2018). For a Salpeter IMF we adopt the average values of $700 M_{\odot} \text{ yr}^{-1}$ and $4 \times 10^8 M_{\odot}$ for SMGs up to redshift 4 reported by Michałowski et al. (2010a). The typical duration of such starbursts can be estimated from the available gas mass available which is of order $10^{11} M_{\odot}$ (Michałowski et al. 2012), i.e., 142 Myr.

A compilation of very high-redshift galaxies was recently provided by Marrone et al. (2018). Below we summarize the observations of galaxies for which sufficient information is available for our purposes.

For the $z = 6.42$ QSO SDSS J1148+525, which has been used as a benchmark in many studies of dust formation at high redshift (Dwek et al. 2007; Gall et al. 2011b; Valiante et al. 2011), the estimated SFR is $3000 M_{\odot} \text{ yr}^{-1}$ (for a Salpeter IMF) and the dust mass is $5.9 \pm 0.7 \times 10^8 M_{\odot}$ (Michałowski et al. 2010b; Gall et al. 2011b). Gall et al. (2011b) quote a starburst age of 30 Myr.

The lensed high-redshift ($z = 6.34$) SMG HFLS3 (Cooray et al. 2014) has an average SFR over 100 Myr of $660 M_{\odot} \text{ yr}^{-1}$ for a Chabrier IMF, corresponding to $1190 M_{\odot} \text{ yr}^{-1}$ for a Salpeter IMF. The measured dust mass is $3 \times 10^8 M_{\odot}$.

Marrone et al. (2018) observed the lensed system SPT0311 at $z = 6.90$, which consists of two separate components, E and W. The respective star-formation rates (Chabrier) are $540 \pm 175 M_{\odot} \text{ yr}^{-1}$ and $2900 \pm 1800 M_{\odot} \text{ yr}^{-1}$, while the inferred dust masses are $0.4 \pm 0.2 \times 10^9 M_{\odot}$ and $2.5 \pm 1.6 \times 10^9 M_{\odot}$. The gas depletion rates are 74 Myr and 93 Myr.

² Adopting a Salpeter IMF (D. Zaritsky, private communication, 2014).

Zavala et al. (2018) observed the $z = 6.03$ lensed dusty galaxy G09 83808. The Salpeter star-formation rate is $640 \pm 90 M_{\odot} \text{ yr}^{-1}$ and the inferred dust mass, based on Herschel observations is $1.9 \pm 0.4 \times 10^8 M_{\odot}$. The gas depletion rate is 40 Myr for a Chabrier IMF.

The three highest redshift galaxies discussed here have lower star-formation rates and classify as LBGs rather than SMGs or ULIRGs. The high-redshift galaxy ($z = 7.5$) was detected with ALMA (Watson et al. 2015). Knudsen et al. (2017) find a current SFR of $13 M_{\odot} \text{ yr}^{-1}$ for a Chabrier IMF. The reported dust mass is $10^{7.7 \pm 0.2} M_{\odot}$. The average star-formation rate over the past 80 Myr is $\sim 49 M_{\odot} \text{ yr}^{-1}$ for a Salpeter IMF (Watson et al. 2015).

Laporte et al. (2017) observed a Y band dropout lensed by the cluster Abell 2744. The galaxy A2744_YD4 has a spectroscopic redshift of $z = 8.38$. ALMA observations indicate a dust mass of $5.5_{-1.7}^{+19.6} \times 10^6 M_{\odot}$ and a star-formation rate of $20.4_{-9.5}^{+17.6} M_{\odot} \text{ yr}^{-1}$ for a Chabrier IMF.

Another Y band dropout Lyman-break galaxy, lensed by the cluster MACS J0416.12403, was recently found to be at a redshift of 8.312 from detection of the [O III] $88 \mu\text{m}$ line in ALMA observations (Tamura et al. 2018). The inferred dust mass is $3.6 \pm 0.7 \times 10^6 M_{\odot}$ (for an assumed dust temperature of 50 K). The star formation rate is $\sim 14 M_{\odot} \text{ yr}^{-1}$ (for a Chabrier IMF) for an age of 180 Myr, with very large uncertainties, depending on the adopted extinction law.

5. RESULTS AND DISCUSSION

In Figure 3 (lower panel) we plot measured dust masses of galaxies against the total dust mass produced by SNe, as estimated from Equation (1). We also show the corresponding dust production rates inferred (Equation 2) in Figure 3 (upper panel). Remarkably, the predictions of the simple model are entirely consistent with the observed dust masses, within the considerable uncertainties over four orders of magnitude and across the redshift range 0–8.4, with dust production rates spanning five orders of magnitudes.

5.1. Mass conservation constraint on maximally dusty galaxies

We have shown that observed dust masses are consistent with being produced by core-collapse SNe at levels similar to those detected in SN 1987A and the Crab, i.e., of order $0.3\text{--}0.4 M_{\odot}$ on average. In this sense, star-forming galaxies may be seen as maximally dusty: they contain the amount of dust SNe can produce, no more and no less. This is equivalent to using the ‘maximum efficiency’ SN dust production models of Gall et al. (2011c), as shown in Figure 2, which assume no subsequent destruction.

The consistency of the maximally dusty model with observed dust masses in star-forming galaxies is remarkable. While it is not proof that the dust is actually produced di-

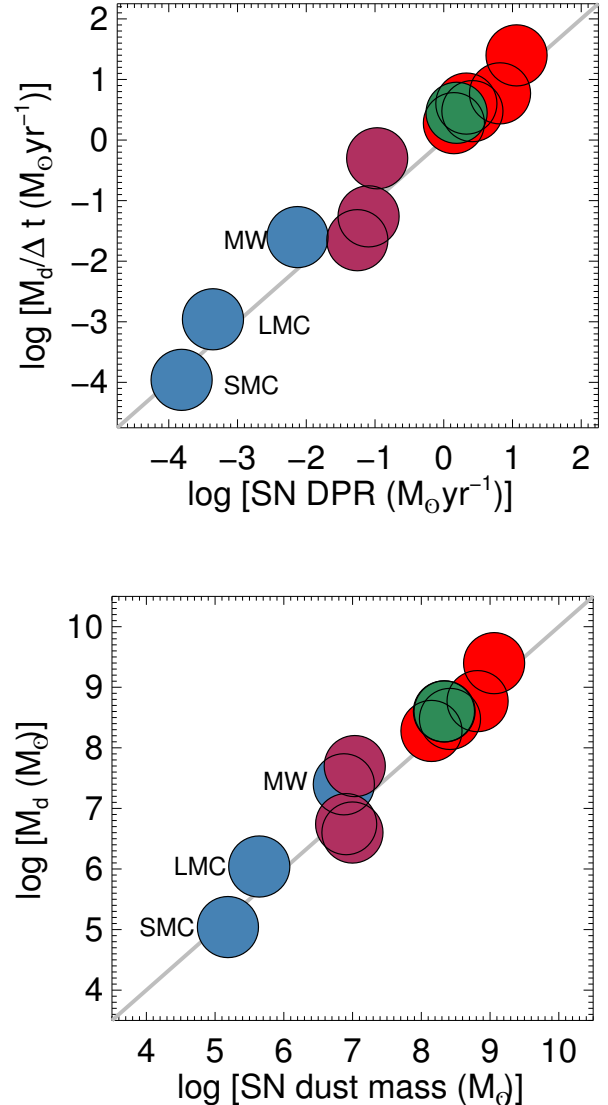


Figure 3. Observationally inferred values versus model predictions, based on Equation (1) and Table 1. A value of $\mu_D = 0.0022$ was adopted for consistency with the use of a Salpeter IMF to infer the observed star-formation rates. Uncertainties are assumed to be 0.4 dex (uncertainties in the DPR have been circularized for simplicity). Blue circles signify Local Group galaxies, the green circle represents intermediate redshift SMGs ($z \sim 2\text{--}3$), the red circles represent high-redshift SMGs ($z \sim 6\text{--}7$), and the purple circles represent the highest redshift Lyman break galaxies ($z \sim 7.5\text{--}8.4$). Lower panel: The model dust masses (Equation 1) are largely consistent with the observed dust masses over four orders of magnitude in dust mass and over the redshift range 0–8.4. Upper panel: The dust production rates (Equation 2) are consistent with the observed values over five orders of magnitude.

rectly in SNe, it sets a strong constraint on models of dust formation in that other dust production mechanisms must obey this mass conservation constraint. For example, if dust is destroyed it must reform in about the same quantities.

5.2. Reformation behind the reverse shock

The main concern in adopting SNe as the dominant dust factories in star-forming galaxies is that the dust could possibly be destroyed shortly after its formation (see Sections 2.2 and 2.3). Regarding destruction by the SN itself we now know that the dust apparently survives and even grows over the first 30 years, as evidenced by the large amounts of ejecta dust in SN 1987A (see Fig. 1). In the coming years we will know if the reverse shock will eventually destroy the dust formed.

On the other hand we also note that while shocks may destroy dust, they might also induce either dust formation, re-formation or re-growth. A classical example where dust re-formation in a SN has been suggested is SN 2008S (Kochanek 2011). Signatures pointing to either dust re-formation or re-growth are seen behind the reverse shock in SN 1987A (M. Matsuura, private communication). Additionally, in Type IIIn SNe, very early dust formation takes place in the cool dense shell, which is formed between the forward and reverse shock in the dense circumstellar medium. Prominent examples are SN 2005ip, 2006jd, 2010jl or 2011ht (e.g., Seale et al. 2012; Humphreys et al. 2012; Gall et al. 2014). A similar mechanism may foster 'in-situ' dust re-formation or re-growth behind a reverse shock penetrating through ejecta dust, in which case the dust budget affected by a reverse shock would be a balance between dust destruction and re-formation. However, theoretical models do not find evidence for dust reformation in the post-reverse shock medium when assuming all dust has been destroyed by the reverse shock in the first place (Biscaro & Cherchneff 2014). Nevertheless, Biscaro & Cherchneff (2014) find that molecules reform and as discussed in Sections 2.2 and 2.3, whether or not dust gets destroyed may depend on the actual grain size distribution of the dust formed in a SN.

5.3. Large grains

As discussed above, from a theoretical point of view, it has been argued that the majority of dust formed in SNe will get destroyed in a reverse shock (Bianchi & Schneider 2007; Mancini et al. 2015; Bocchio et al. 2016) while others find a much smaller effect (Nozawa et al. 2007). The differences in the destruction efficiency of dust grains by SN reverse shocks can be traced back to the strong sensitivity to the markedly different initial grain size distributions, e.g., resulting from these models (Todini & Ferrara 2001; Nozawa et al. 2003). Similarly, variations in destruction time scales and efficiencies of ISM dust through SN shocks are also subject to the

grain sizes considered (see Section 2.3). Simulations and models of dust reprocessing of dust grains through shocks indicate that large fractions can survive (Silvia et al. 2010), especially if grains are large ($> 0.1\mu\text{m}$) (Slavin et al. 2004; Biscaro & Cherchneff 2016). Recent observations suggest the formation of a significant amount of large grains. From the extinction curve of dust formed in the Type IIIn SN 2010jl, Gall et al. (2014) inferred the formation of large grains. Subsequently, this was also inferred from detailed modelling of the dust formed in SN 1987A and the Crab (Owen & Barlow 2015; Wesson et al. 2015; Bevan & Barlow 2016). Bak Nielsen et al. (2018) also recently found that the extinction curve of dust formed in the Type IIIn SN 2005ip might be interpreted as being due to the formation of large grains. The formation of large grains in SNe is backed by theoretical models (Sarangi & Cherchneff 2015) and by the observations of shallow extinction curves in strongly star-forming regions (De Marchi et al. 2016).

5.4. Current state of affairs

Under the assumption of efficient SN reverse shock dust destruction, one is driven to advocate accretion in the ISM to re-grow dust grains (Draine 2009; Michałowski 2015; Mancini et al. 2015) (AGB stars are not efficient dust producers on short time scales, i.e., at high redshift (Gall et al. 2011b)). This process may be efficient in a MW environment, but Mancini et al. (2015) suggested from chemical evolution models that the accretion time scale in high-redshift galaxies must be about 200,000 yr. Such a short time scale³ sets some stringent constraints on this scenario.

While the original suggestion was that accretion would occur in the cold neutral medium (CNM; $n \sim 10\text{--}100\text{ cm}^{-3}$) (Draine 2009) it has been customary to assume that the main growth site in high-redshift galaxies is in molecular clouds at a much higher density ($> 10^4\text{ cm}^{-3}$). However, as demonstrated by Ferrara et al. (2016) (see discussion in Section 2.4), grain growth cannot happen efficiently in molecular clouds of high density, hence one needs to reconsider the CNM (Draine 2009; Zhukovska et al. 2016; Ferrara et al. 2016). In this case, the density is 2–3 orders of magnitude lower than in molecular clouds. As the accretion time scale is proportional to a/n (Asano et al. 2013; Ferrara et al. 2016), where a is the grain size, this requires grains that are smaller by 2–3 orders of magnitude, in order to provide the needed increased grain surface area. Therefore, nm-sized grains are required to be able to reach sufficiently short growth time scales at high redshift. Such small grains pose severe challenges (Zhukovska

³ We note that in chemical evolution models (see Section 3), the entire evolution of a SN remnant is considered 'instant'. On the other hand, as discussed in Section 2.4, the mixing of elements into the ISM may take many Myr.

et al. 2018). In particular, the temperatures of such small grains will be so high, especially considering the high CMB temperature at high redshift, that accreted ions will not stick to the grains (Ferrara et al. 2016).

Alternatively, dust reformation and growth could happen on an even faster time scale, immediately after dust destruction, e.g., behind the reverse shock of the SN (Section 5.2). The constraint from our model is that the different scenarios (SN dust formation, reverse shock re-formation, or interstellar grain growth) must reach the same level of net dust production per SN. Given that interstellar destruction processes due to SN forward shocks or ablation apply to any kind of dust, the need for limited destruction in high-redshift galaxies (Gall et al. 2011b; Hjorth et al. 2014) applies to any of these scenarios. This might favour processes which can produce large grains.

5.5. Summary

We have gathered recent observational and theoretical results on SN dust formation and dust content in Local Group and high-redshift galaxies. The observed dust masses can be accounted for by a simple unifying model in which the majority of the dust is formed by SNe in the current star-formation episode. The model does not rule out other dust production scenarios but they are not strongly required either. It seems likely that if SNe produce the majority of the dust in massive high-redshift galaxies, they are also important sources of dust in Local Group galaxies.

We have not specified exactly how the dust must ultimately be produced, such as, e.g., in the SN ejecta. The only assumption is that the dust is formed by SNe or massive stars on a short time scale, i.e., $\lesssim 10\text{--}100$ Myr. For example, significant dust could have been produced in mass loss events prior to the SN explosion (or fall-back black hole formation), or dust may have been formed in rapid grain growth scenarios out of the metals expelled by the massive star or SN. Rapid destruction and re-formation of the dust is of course also allowed, as long as the two terms are roughly balanced (Dwek 1998).

We conclude that the amount of dust in star-forming galaxies is consistent with having been produced by SNe. Moreover, what has been destroyed must have reformed rapidly.

We thank Sebastian Hönig and Mikako Matsuura for helpful comments and suggestions. C.G. acknowledges funding by the Carlsberg Foundation. J.H. was supported by a VILLUM FONDEN Investigator grant (project number 16599).

REFERENCES

- Aoyama, S., Hou, K.-C., Hirashita, H., Nagamine, K., & Shimizu, I. 2018, *MNRAS*, [arXiv:1802.04027](#)
- Arendt, R. G., Dwek, E., Kober, G., Rho, J., & Hwang, U. 2014, *ApJ*, **786**, 55
- Arendt, R. G., Dwek, E., Blair, W. P., et al. 2010, *ApJ*, **725**, 585
- Asano, R. S., Takeuchi, T. T., Hirashita, H., & Inoue, A. K. 2013, *Earth, Planets, and Space*, **65**, 213
- Baba, J., Morokuma-Matsui, K., & Saitoh, T. R. 2017, *MNRAS*, **464**, 246
- Bak Nielsen, A.-S., Hjorth, J., & Gall, C. 2018, ArXiv e-prints, [arXiv:1801.04217 \[astro-ph.SR\]](#)
- Barlow, M. J. 1978, *MNRAS*, **183**, 367
- Barlow, M. J., Sugerman, B. E. K., Fabbri, J., et al. 2005, *ApJL*, **627**, L113
- Barlow, M. J., Krause, O., Swinyard, B. M., et al. 2010, *A&A*, **518**, L138
- Bevan, A., & Barlow, M. J. 2016, *MNRAS*, **456**, 1269
- Bevan, A., Barlow, M. J., & Milisavljevic, D. 2017, *MNRAS*, **465**, 4044
- Bianchi, S., & Schneider, R. 2007, *MNRAS*, **378**, 973
- Biscaro, C., & Cherchneff, I. 2014, *A&A*, **564**, A25
- . 2016, *A&A*, **589**, A132
- Bocchio, M., Marassi, S., Schneider, R., et al. 2016, *A&A*, **587**, A157
- Bolato, A. D., Leroy, A. K., Jameson, K., et al. 2011, *ApJ*, **741**, 12
- Boogert, A. C. A., Chiar, J. E., Knez, C., et al. 2013, *ApJ*, **777**, 73
- Boogert, A. C. A., Gerakines, P. A., & Whittet, D. C. B. 2015, *ARA&A*, **53**, 541
- Bot, C., Ysard, N., Paradis, D., et al. 2010, *A&A*, **523**, A20
- Boyer, M. L., Srinivasan, S., Riebel, D., et al. 2012, *ApJ*, **748**, 40
- Calura, F., Gilli, R., Vignali, C., et al. 2014, *MNRAS*, **438**, 2765
- Calura, F., Pipino, A., & Matteucci, F. 2008, *A&A*, **479**, 669
- Caselli, P., & Ceccarelli, C. 2012, *A&A Rv*, **20**, 56
- Ceccarelli, C., Viti, S., Balucani, N., & Taquet, V. 2018, *MNRAS*, **476**, 1371
- Cernuschi, F., Marsicano, F., & Codina, S. 1967, *Annales d'Astrophysique*, **30**, 1039
- Ceverino, D., Klessen, R., & Glover, S. 2018, ArXiv e-prints, [arXiv:1801.10382](#)
- Cherchneff, I., & Dwek, E. 2010, *ApJ*, **713**, 1
- Chevalier, R. A. 1977, *ARA&A*, **15**, 175
- Chomiuk, L., & Povich, M. S. 2011, *AJ*, **142**, 197
- Clayton, D. D. 1979, *Ap&SS*, **65**, 179
- Cooray, A., Calanog, J., Wardlow, J. L., et al. 2014, *ApJ*, **790**, 40
- de Avillez, M. A., & Mac Low, M.-M. 2002, *ApJ*, **581**, 1047
- De Cia, A., Ledoux, C., Mattsson, L., et al. 2016, *A&A*, **596**, A97
- De Looze, I., Barlow, M. J., Swinyard, B. M., et al. 2017, *MNRAS*, **465**, 3309
- De Marchi, G., Panagia, N., Sabbi, E., et al. 2016, *MNRAS*, **455**, 4373
- Dobbs, C. L., & Pringle, J. E. 2013, *MNRAS*, **432**, 653
- Dopita, M. A., Seitzzahl, I. R., Sutherland, R. S., et al. 2016, *ApJ*, **826**, 150
- Draine, B. T. 2009, in *Astronomical Society of the Pacific Conference Series*, Vol. 414, *Cosmic Dust - Near and Far*, ed. T. Henning, E. Grün, & J. Steinacker, 453
- Dunne, L., Eales, S., Ivison, R., Morgan, H., & Edmunds, M. 2003, *Nature*, **424**, 285
- Dunne, L., Maddox, S. J., Ivison, R. J., et al. 2009, *MNRAS*, **394**, 1307
- Dwek, E. 1998, *ApJ*, **501**, 643
- . 2016, *ApJ*, **825**, 136
- Dwek, E., & Arendt, R. G. 2015, *ApJ*, **810**, 75
- Dwek, E., Galliano, F., & Jones, A. P. 2007, *ApJ*, **662**, 927
- Ferrara, A., Viti, S., & Ceccarelli, C. 2016, *MNRAS*, **463**, L112
- Fox, O., Skrutskie, M. F., Chevalier, R. A., et al. 2009, *ApJ*, **691**, 650
- France, K., McCray, R., Penton, S. V., et al. 2011, *ApJ*, **743**, 186
- Fransson, C., Larsson, J., Spyromilio, J., et al. 2013, *ApJ*, **768**, 88
- Fry, B. J., Fields, B. D., & Ellis, J. R. 2018, ArXiv e-prints, [arXiv:1801.06859 \[astro-ph.HE\]](#)
- Gall, C., Andersen, A. C., & Hjorth, J. 2011a, *A&A*, **528**, A13
- . 2011b, *A&A*, **528**, A14
- Gall, C., Hjorth, J., & Andersen, A. C. 2011c, *A&A Rv*, **19**, 43
- Gall, C., Hjorth, J., Watson, D., et al. 2014, *Nature*, **511**, 326
- Ghavamian, P., & Williams, B. J. 2016, *ApJ*, **831**, 188
- Ginolfi, M., Graziani, L., Schneider, R., et al. 2018, *MNRAS*, **473**, 4538
- Gomez, H. L., Vlahakis, C., Stretch, C. M., et al. 2010, *MNRAS*, **401**, L48
- Gomez, H. L., Dunne, L., Ivison, R. J., et al. 2009, *MNRAS*, **397**, 1621
- Gomez, H. L., Krause, O., Barlow, M. J., et al. 2012, *ApJ*, **760**, 96
- Harris, J., & Zaritsky, D. 2004, *AJ*, **127**, 1531
- . 2009, *AJ*, **138**, 1243
- Heger, A., Fryer, C. L., Woosley, S. E., Langer, N., & Hartmann, D. H. 2003, *ApJ*, **591**, 288
- Hirashita, H. 2012, *MNRAS*, **422**, 1263
- Hjorth, J., Gall, C., & Michałowski, M. J. 2014, *ApJL*, **782**, L23
- Hopkins, P. F., & Squire, J. 2018, ArXiv e-prints, [arXiv:1801.10166](#)
- Hoyle, F., & Wickramasinghe, N. C. 1970, *Nature*, **226**, 62
- Humphreys, R. M., Davidson, K., Jones, T. J., et al. 2012, *ApJ*, **760**, 93
- Ibeling, D., & Heger, A. 2013, *ApJL*, **765**, L43
- Indebetouw, R., Matsuura, M., Dwek, E., et al. 2014, *ApJL*, **782**, L2

- Jenkins, E. B. 2009, *ApJ*, 700, 1299
- Jones, A. P., & Nuth, J. A. 2011, *A&A*, 530, A44
- Jones, A. P., Tielens, A. G. G. M., & Hollenbach, D. J. 1996, *ApJ*, 469, 740
- Knudsen, K. K., Watson, D., Frayer, D., et al. 2017, *MNRAS*, 466, 138
- Kochanek, C. S. 2011, *ApJ*, 743, 73
- Kotak, R., Meikle, W. P. S., Farrah, D., et al. 2009, *ApJ*, 704, 306
- Kozasa, T., Hasegawa, H., & Nomoto, K. 1989, *ApJ*, 344, 325
- Krumholz, M. R., & Ting, Y.-S. 2018, *MNRAS*, 475, 2236
- Lakićević, M., van Loon, J. T., Meixner, M., et al. 2015, *ApJ*, 799, 50
- Laporte, N., Ellis, R. S., Boone, F., et al. 2017, *ApJL*, 837, L21
- Lau, R. M., Herter, T. L., Morris, M. R., Li, Z., & Adams, J. D. 2015, *Science*, 348, 413
- Lawrence, A. 2012, *MNRAS*, 423, 451
- Leroy, A., Bolatto, A., Stanimirovic, S., et al. 2007, *ApJ*, 658, 1027
- Madau, P., & Dickinson, M. 2014, *ARA&A*, 52, 415
- Mancini, M., Schneider, R., Graziani, L., et al. 2015, *MNRAS*, 451, L70
- Marrone, D. P., Spilker, J. S., Hayward, C. C., et al. 2018, *Nature*, 553, 51
- Martínez-González, S., Wunsch, R., Palouš, J., et al. 2018, *ArXiv e-prints*, [arXiv:1808.06614](https://arxiv.org/abs/1808.06614)
- Matsuura, M., Woods, P. M., & Owen, P. J. 2013, *MNRAS*, 429, 2527
- Matsuura, M., Barlow, M. J., Zijlstra, A. A., et al. 2009, *MNRAS*, 396, 918
- Matsuura, M., Dwek, E., Meixner, M., et al. 2011, *Science*, 333, 1258
- Matsuura, M., Dwek, E., Barlow, M. J., et al. 2015, *ApJ*, 800, 50
- Mattila, S., Meikle, W. P. S., Lundqvist, P., et al. 2008, *MNRAS*, 389, 141
- Mattsson, L., Gomez, H. L., Andersen, A. C., & Matsuura, M. 2015, *MNRAS*, 449, 4079
- Mauerhan, J., & Smith, N. 2012, *MNRAS*, 424, 2659
- McKinnon, R., Torrey, P., & Vogelsberger, M. 2016, *MNRAS*, 457, 3775
- McKinnon, R., Torrey, P., Vogelsberger, M., Hayward, C. C., & Marinacci, F. 2017, *MNRAS*, 468, 1505
- Meikle, W. P. S., Kotak, R., Farrah, D., et al. 2011, *ApJ*, 732, 109
- Meixner, M., Panuzzo, P., Roman-Duval, J., et al. 2013, *AJ*, 146, 62
- Micelotta, E. R., Dwek, E., & Slavin, J. D. 2016, *A&A*, 590, A65
- Micelotta, E. R., Matsuura, M., & Sarangi, A. 2018, *SSRv*, 214, 53
- Michałowski, M., Hjorth, J., & Watson, D. 2010a, *A&A*, 514, A67
- Michałowski, M. J. 2015, *A&A*, 577, A80
- Michałowski, M. J., Dunlop, J. S., Cirasuolo, M., et al. 2012, *A&A*, 541, A85
- Michałowski, M. J., Murphy, E. J., Hjorth, J., et al. 2010b, *A&A*, 522, A15
- Michałowski, M. J., Watson, D., & Hjorth, J. 2010c, *ApJ*, 712, 942
- Milisavljevic, D., Fesen, R. A., Chevalier, R. A., et al. 2012, *ApJ*, 751, 25
- Morris, P. W., Gull, T. R., Hillier, D. J., et al. 2017, *ApJ*, 842, 79
- Morse, J. A., Fesen, R. A., Chevalier, R. A., et al. 2004, *ApJ*, 614, 727
- Nath, B. B., Laskar, T., & Shull, J. M. 2008, *ApJ*, 682, 1055
- Nittler, L. R., O'D. Alexander, C. M., Liu, N., & Wang, J. 2018, *ApJL*, 856, L24
- Nozawa, T., Kozasa, T., Habe, A., et al. 2007, *ApJ*, 666, 955
- Nozawa, T., Kozasa, T., Umeda, H., Maeda, K., & Nomoto, K. 2003, *ApJ*, 598, 785
- Ormel, C. W., Paszun, D., Dominik, C., & Tielens, A. G. G. M. 2009, *A&A*, 502, 845
- Otsuka, M., van Loon, J. T., Long, K. S., et al. 2010, *A&A*, 518, L139
- Owen, P. J., & Barlow, M. J. 2015, *ApJ*, 801, 141
- Petit, A. C., Krumholz, M. R., Goldbaum, N. J., & Forbes, J. C. 2015, *MNRAS*, 449, 2588
- Pipino, A., Fan, X. L., Matteucci, F., et al. 2011, *A&A*, 525, A61
- Popping, G., Somerville, R. S., & Galametz, M. 2017, *MNRAS*, 471, 3152
- Pozzo, M., Meikle, W. P. S., Fassia, A., et al. 2004, *MNRAS*, 352, 457
- Rho, J., Gomez, H. L., Boogert, A., et al. 2017, *ArXiv e-prints*, [arXiv:1707.08230](https://arxiv.org/abs/1707.08230)
- Rho, J., Reach, W. T., Tappe, A., et al. 2009, *ApJ*, 700, 579
- Rowlands, K., Gomez, H. L., Dunne, L., et al. 2014, *MNRAS*, 441, 1040
- Sankrit, R., Williams, B. J., Borkowski, K. J., et al. 2010, *ApJ*, 712, 1092
- Sarangi, A., & Cherchneff, I. 2013, *ApJ*, 776, 107
- , 2015, *A&A*, 575, A95
- Schneider, R., Valiante, R., Ventura, P., et al. 2014, *MNRAS*, 442, 1440
- Seale, J. P., Looney, L. W., Wong, T., et al. 2012, *ApJ*, 751, 42
- Silvia, D. W., Smith, B. D., & Shull, J. M. 2010, *ApJ*, 715, 1575
- , 2012, *ApJ*, 748, 12
- Skibba, R. A., Engelbracht, C. W., Aniano, G., et al. 2012, *ApJ*, 761, 42
- Slavin, J. D., Dwek, E., & Jones, A. P. 2015, *ApJ*, 803, 7
- Slavin, J. D., Jones, A. P., & Tielens, A. G. G. M. 2004, *ApJ*, 614, 796
- Smith, N. 2012, in *Astrophysics and Space Science Library*, Vol. 384, *Eta Carinae and the Supernova Impostors*, ed. K. Davidson & R. M. Humphreys, 145
- Smith, N., Foley, R. J., & Filippenko, A. V. 2008, *ApJ*, 680, 568

- Sonneborn, G., Pun, C. S. J., Kimble, R. A., et al. 1998, *ApJL*, 492, L139
- Strolger, L.-G., Dahlen, T., Rodney, S. A., et al. 2015, *ApJ*, 813, 93
- Tamura, Y., Mawatari, K., Hashimoto, T., et al. 2018, ArXiv e-prints, [arXiv:1806.04132](https://arxiv.org/abs/1806.04132)
- Temim, T., & Dwek, E. 2013, *ApJ*, 774, 8
- Temim, T., Dwek, E., Arendt, R. G., et al. 2017, *ApJ*, 836, 129
- Temim, T., Dwek, E., Tchernyshyov, K., et al. 2015, *ApJ*, 799, 158
- Tielens, A. G. G. M. 1998, *ApJ*, 499, 267
- Todini, P., & Ferrara, A. 2001, *MNRAS*, 325, 726
- Truelove, J. K., & McKee, C. F. 1999, *ApJS*, 120, 299
- Umeda, H., & Nomoto, K. 2002, *ApJ*, 565, 385
- Valiante, R., Schneider, R., Salvadori, S., & Bianchi, S. 2011, *MNRAS*, 416, 1916
- Wallström, S. H. J., Biscaro, C., Salgado, F., et al. 2013, *A&A*, 558, L2
- Wang, R., Carilli, C. L., Wagg, J., et al. 2008, *ApJ*, 687, 848
- Watson, D., Christensen, L., Knudsen, K. K., et al. 2015, *Nature*, 519, 327
- Wesson, R., Barlow, M. J., Matsuura, M., & Ercolano, B. 2015, *MNRAS*, 446, 2089
- Whalen, D. J., Even, W., Lovekin, C. C., et al. 2013, *ApJ*, 768, 195
- Winkler, P. F., Hamilton, A. J. S., Long, K. S., & Fesen, R. A. 2011, *ApJ*, 742, 80
- Wooden, D. H., Rank, D. M., Bregman, J. D., et al. 1993, *ApJS*, 88, 477
- Woosley, S. E., & Weaver, T. A. 1995, *ApJS*, 101, 181
- Zavala, J. A., Montaña, A., Hughes, D. H., et al. 2018, *Nature Astronomy*, 2, 56
- Zhukovska, S., Dobbs, C., Jenkins, E. B., & Klessen, R. S. 2016, *ApJ*, 831, 147
- Zhukovska, S., Gail, H.-P., & Tieloff, M. 2008, *A&A*, 479, 453
- Zhukovska, S., Henning, T., & Dobbs, C. 2018, *ApJ*, 857, 94